

ORIGINAL ARTICLE

ENDOSCOPY

doi.org/10.1590/S0004-2803.246102023-62

Early stages of colorectal cancer characterization by autofluorescence 3D microscopy: a preliminary study

Luciana Ariadna **ERBES**^{1,2}, Víctor Hugo **CASCO**^{1,2} and Javier **ADUR**^{1,2}

¹ Universidad Nacional de Entre Ríos, Facultad de Ingeniería, Laboratorio de Microscopía Aplicada a Estudios Moleculares y Celulares. Oro Verde, Argentina. ² Consejo Nacional de Investigaciones Científicas y Técnicas, Instituto de Investigación y Desarrollo en Bioingeniería y Bioinformática. Oro Verde, Argentina.

HIGHLIGHTS

- A new digital image processing method was developed to measure intensity in 3D autofluorescence images of colorectal samples using a CRC mouse model.
- This method showed that autofluorescence intensity in colon mucosa is similar in healthy tissue but changes significantly in tumor development.
- Statistical analysis revealed CRC traits detectable from the second week post-induction, aiding in early CRC detection.
- The study provides a basis for 3D autofluorescence characterization in colorectal tissue from dysplasia to cancer, although variability in autofluorescence limits data systematization during cancer progression.

Received: 14 April 2023
Accepted: 8 August 2023

Declared conflict of interest of all authors: none
Disclosure of funding: This work was supported by a PIO CONICET-UNER grant: 4337/15; N°: N8 14620140100004 CO.
Declaration of use of artificial intelligence: none
Corresponding author: Javier Adur.
E-mail: javier.adur@uner.edu.ar



ABSTRACT – Background – Colorectal cancer is one of the most prevalent pathologies worldwide whose prognosis is linked to early detection. Colonoscopy is the gold standard for screening, and diagnosis is usually made histologically from biopsies. Aiming to reduce the inspection and diagnostic time as well as the biopsies and resources involved, other techniques are being promoted to conduct accurate in vivo colonoscopy assessments. Optical biopsy aims to detect normal and neoplastic tissues analysing the autofluorescence spectrum based on the changes in the distribution and concentration of autofluorescent molecules caused by colorectal cancer. Therefore, the autofluorescence contribution analysed by image processing techniques could be an approach to a faster characterization of the target tissue. **Objective** – Quantify intensity parameters through digital processing of two data sets of three-dimensional wide-field autofluorescence microscopy images, acquired by fresh colon tissue samples from a colorectal cancer murine model. Additionally, analyse the autofluorescence data to provide a characterization over a volume of approximately 50 µm of the colon mucosa for each image, at second (2nd), fourth (4th) and eighth (8th) weeks after colorectal cancer induction. **Methods** – Development of a colorectal cancer murine model using azoxymethane/dextran sodium sulphate induction, and data sets acquisition of Z-stack images by widefield autofluorescence microscopy, from control and colorectal cancer induced animals. Pre-processing steps of intensity value adjustments followed by quantification and characterization procedures using image processing workflow automation by Fiji's macros, and statistical data analysis. **Results** – The effectiveness of the colorectal cancer induction model was corroborated by a histological assessment to correlate and validate the link between histological and autofluorescence changes. The image digital processing methodology proposed was then performed on the three-dimensional images from control mice and from the 2nd, 4th, and 8th weeks after colorectal cancer chemi-

cal induction, for each data set. Statistical analyses found significant differences in the mean, standard deviation, and minimum parameters between control samples and those of the 2nd week after induction with respect to the 4th week of the first experimental study. This suggests that the characteristics of colorectal cancer can be detected after the 2nd week post-induction. **Conclusion** – The use of autofluorescence still exhibits levels of variability that prevent greater systematization of the data obtained during the progression of colorectal cancer. However, these preliminary outcomes could be considered an approach to the three-dimensional characterization of the autofluorescence of colorectal tissue, describing the autofluorescence features of samples coming from dysplasia to colorectal cancer.

Keywords – Autofluorescence; colorectal cancer; image processing; microscopy.

INTRODUCTION

Colorectal cancer (CRC), a leading cause of death worldwide, is a highly aggressive disease with a high metastatic potential^(1,2) and it primarily arises from adenomas. The disease exhibits slow development over more than 10 years through the adenoma-carcinoma sequence^(3,4).

Colonoscopy is considered the gold standard for CRC screening, being the most used tool for early detection and the resection of pre-neoplastic lesions, aiming to timely interrupt the adenoma-carcinoma sequence^(4,5). Even though diagnosis is usually made histologically from the biopsy samples taken during endoscopy, advanced endoscopic imaging techniques improve the accuracy beyond what is afforded by conventional white light imaging. They provide a more detailed visualization of the mucosa by enhancing morphology^(3,4,6). Thus, the images generated by this emerging generation of endoscopic imaging technologies would have the potential to act as an “optical biopsy” to aid clinical decision-making⁽⁷⁾.

Autofluorescence images (AFI) are used for polyp differentiation based on the analysis of the autofluorescence spectra, as changes are observed between adenomas and normal mucosa because of the biochemical and morphological tissue alterations during cancerous transformation^(8,9). In this manner, endogenous fluorophores and their role as intrinsic biomarkers offer an exceptionally powerful tool for characterizing, in real time, even subtle changes of interconnected morphological and metabolic properties of cells and tissues under physiological or altered conditions⁽¹⁰⁾. In particular, CRC is known to cause changes in the concentration and distribution of autofluorescent molecules, such as collagen, elastin,

flavin adenine dinucleotide (FAD), nicotinamide adenine dinucleotide (NADH), protoporphyrin IX (PPIX) and lysosome granules^(11,12).

The use of autofluorescence has been reported as a means of characterizing colorectal lesions at screening stages or from resections^(6,8,12,13-16). However, the AFI performance could be affected by low-quality imaging and a highly variable level of background fluorescence among patients^(8,17). Even more, as the luminal surface fluorescence and the use of autofluorescence to detect early cancers or premalignant lesions depend on tissue architecture and biochemical composition⁽¹⁴⁾, a good understanding of the fluorescence properties of each endogenous chromophore and their change upon observation condition is required to use autofluorescence for biomedical studies and medical diagnostics⁽¹⁸⁾.

Finally, as previously exposed, the differentiation of neoplastic and normal colon tissues by autofluorescence remains a challenge for the detection and diagnosis of CRC and its precursors⁽¹¹⁾. Thus, research advances in autofluorescence characterization and computer-aided diagnostic approaches could help to establish it as a stand-alone diagnosis technique during in vivo fluorescence endoscopy, or at least, to complement the current criteria, bypassing staining techniques and decreasing the number of biopsies required, as well as the resources and time involved in the inspection.

METHODS

This section describes the CRC murine model used and the samples, the features of the acquired images and optical system, the image digital processing methodology proposed, and the statistical methods selected for the analyses.

CRC murine model and samples

Two experimental studies were performed using adult male BALB/cCmedc strain mice (n=24 for each time) ranging from 17 to 26 g. Both included a random assignment to control and CRC-induced animals. The latter group of mice was intraperitoneally injected with 10 mg/kg azoxymethane (AOM; Santa Cruz) on day zero, and one week later, they were treated with dextran sodium sulphate (DSS; MP Biomedicals, Solon, OH, USA) administered in the drinking water for 7 days. This procedure was performed following the method described by Rosenberg et al.⁽¹⁹⁾ and previously validated in Erbes et al.⁽²⁰⁾. The control group of mice was saline injected on day zero, and it was provided with drinking water without DSS. Mice were sacrificed by cervical dislocation, and distal colon segments were extracted from the control mice at day zero and from the AOM-injected mice at second (2nd), fourth (4th), and eighth (8th) weeks after the injection.

The samples were longitudinally sectioned while being kept on ice and wetted with saline. After this process, the samples were mounted on cover slipped slides, with the luminal surface placed upwards for immediate observation under fluorescence microscopy. For the CRC induction assessment, a Leica microscope was used to conduct an optical microscopy examination on 5 µm thick hematoxylin-eosin-stained sections (H&E) obtained from paraffin-embedded samples following a standard histological procedure. A blinded review was conducted by an experienced pathologist.

The use of laboratory animals was conducted in accordance with the principles set forth in the Guide for the Care and Use of Laboratory Animals⁽²¹⁾. Furthermore, all animal work and care were conducted following the guidelines approved by the CONICET directory and the UNER for PIO grant: 43337/15. Procedures were carried out at the laboratories in the FI-UNER, with all efforts made to minimize animal suffering.

Image acquisition

Z-stack images (70 optical sections: 1920×1440 pixel image, 0.72 µm z-step size) were acquired by optical sectioning using an Olympus IX83 inverted microscope (Olympus, Tokyo, Japan). The microscope was equipped with a 20X/0.75 NA objective lens

(UPLSAPO, Olympus), a fluorescence illumination source (U-HGLGPS, Olympus), a fluorescence filter cube (U-3N41001, exciter: BP HQ 460-500, dichroic: Q505LP, emitter: BP 510-560) and a high-sensitivity digital camera based on a CMOS image sensor (3.63 µm/pixel, ORCA Flash 2.8, Hamamatsu, Japan) with 0.5X magnification lens.

H&E images (4288x3216 pixel image) were registered using a Leica microscope (Leica Microsystems). The microscope was equipped with a 25X/0.5 NA objective lens and a digital camera (14 mp, Olympus VG-140).

Image digital processing methodology

Fiji⁽²²⁾ macros were developed for automating the image processing workflow, primarily involving procedures of intensity value adjustments, and quantification. These macros were applied uniformly in both experimental studies, and their detailed steps are described in the following subsections.

Pre-processing steps

The photobleaching and out-of-focus fluorescence effects were reduced by applying the Exponential Fit Correction Method from the Bleach Correction plugin⁽²³⁾ followed by five deconvolution iterations of the algorithm Richardson-Lucy (RL) from the DeconvolutionLab plugin⁽²⁴⁾, with a reflective Boundary Condition. A theoretical point spread function (PSF) generated by the Widefield Fluorescence Microscope PSF plugin⁽²⁵⁾ available in Icy⁽²⁶⁾ was used.

Quantification method

The three-dimensional (3D) autofluorescence quantification process began with an initial step of adjusting intensity values over the pre-processed image to standardize the quantification conditions, considering the use of automatic exposure times in the image acquisition. Thus, the proposed and patented method of Pang et al.^(27,28) was applied to scale pixel intensities, required when comparing grayscale images acquired at different exposure times.

As FIGURE 1 summarizes, the adjusted intensity (Intensity(t1)) was determined using a reference exposure time (t1), the intensity value of the image to be processed (Intensity(t2)) and its exposure time (t2). Additionally, the calculation involved consider-

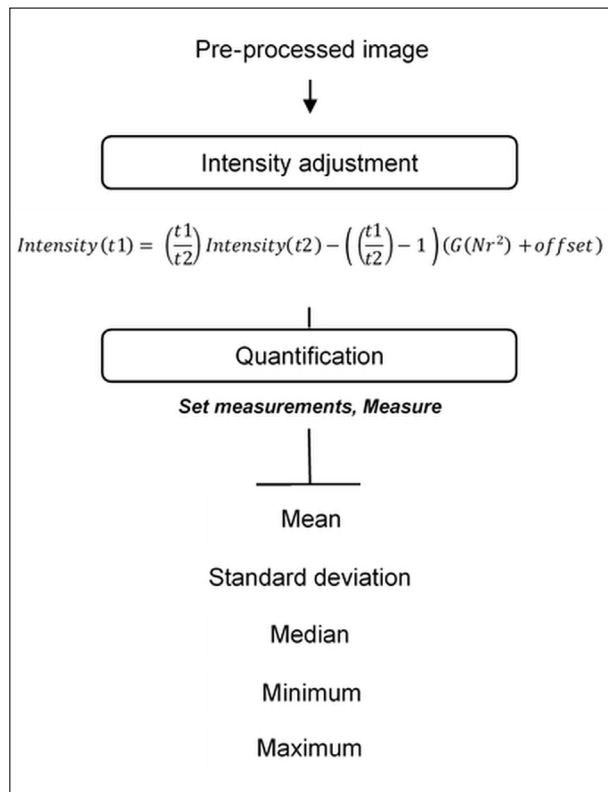


FIGURE 1. Intensity adjustment and quantification method workflow.

ring the camera's readout noise ($Nr=3$ electron/pixel), gain ($G=1$), and offset (0). All of these values were set based on a reference image, and the configuration specifications and the technical note of the camera⁽²⁹⁾. Subsequently, intensity parameters, such as mean, standard deviation (SD), median, minimum, and maximum, were quantified using the Measure tool available in Fiji's Analyze Menu⁽³⁰⁾.

Autofluorescence characterization

The 3D autofluorescence spanning approximately $50\ \mu\text{m}$ of tissue thickness, from the luminal surface of the colonic mucosal layer to the inner, was described by the median, interquartile range, mean, and SD of the intensity parameters for each point of time from both experimental studies. The analysed extension includes the intensities present in the tissue where the upper third of non-neoplastic pits for distal colonic crypts from mice can be found, following the report of Tan et al.⁽³¹⁾. This additional information complements and supports the morphological characterization, aiding in differentiating colorectal neoplastic from non-neoplastic features.

Statistics

Kruskal-Wallis tests were carried out to assess the differences in intensity parameters between the control, 2nd, 4th, and 8th weeks for each experimental study. The quantified data used for the analysis were obtained from 3D images belonging to one sample from three to six mice for each time point (the number of quantified images used for each one is detailed in TABLE 1). When the results were significant, Mann-Whitney tests were applied followed by a p-value Holm correction. The analyses were conducted in RStudio⁽³²⁾ and P-values <0.05 and <0.01 were considered statistically significant.

RESULTS

Histological assessment of the CRC induction

Distal colon sections were blind-analysed by the H&E staining gold standard method to assess the reproducibility of the AOM/DSS induction and CRC development phases. Histological morphology confirmed the effectiveness of the CRC induction model, as evidenced by progressive alterations in morphology and arrangement of the crypts, consistent with the multi-step sequence of dysplasia-adenoma-carcinoma. Consequently, the links between histological and autofluorescence changes in the data sets can be correlated and validated.

FIGURE 2 exemplifies such a correlation and provide evidence of CRC induction. Whereas uniformly arranged round-shaped pits are presented in the mucosa cross-sections of control samples, the alterations exhibited by the AOM/DSS induced ones correlate with the progression from dysplasia to CRC. Loss of sphericity, reduction of arrangement regularity and connective tissue changes are features in progress from the 2nd to the 8th weeks of induction, showing a mixture of variable size morphologies as round, oval, and star-like pits. Starting from the 4th week, noticeable mucosa structural distortions are observed, characterized by aberrant crypt foci and adenomas. By the 8th week the mucosa exhibits adenocarcinoma and infiltration of lymphoid tissue. Supporting the previously mentioned descriptions, different levels of altered epithelial architecture and leukocyte infiltration as signs of inflammation, as well as loss of rectilinear

TABLE 1. 3D quantification data of autofluorescence intensity.

Time Point	Study (N°)	3D Image (N°)	Mean	SD	Median	Minimum	Maximum
Zero day (Control)	1	4	1,322.67 (1,189.98/1,398.58)	130.19 (101.77/159.63)	1,319.55 (1,173.34/1,418.18)	782.69 (722.38/808.25)	2,563.58 (1,975.06/3,489.14)
	2	5	1,303.93 (1,219.74/1,597.20)	169.23 (115.81/200.57)	1,316.06 (1,220.70/1,622.61)	708.94 (619.50/776.33)	2,922.03 (2,462.98/3,035.42)
2nd week	1	5	1,037.04 (954.95/1,433.84)	93.67 (70.17/106.08)	1,037.60 (964.24/1,434.65)	649.21 (586.80/912.16)	2,610.02 (1,549.37/2,638.99)
	2		1,311.73 (1,006.33/1,314.44)	95.80 (90.14/118.77)	1,307.36 (1,003.53/1,320.40)	787.51 (567.49/959.09)	2,152.05 (1,975.97/2,586.98)
4th week	1	6	3,135.84 (2,957.97/3,245.52)	357.46 (299.49/378.69)	3,159.46 (2,994.03/3,258.40)	1,711.36 (1,566.76/1,928.51)	6,247.33 (5,165.51/8,702.67)
	2		1,454.33 (1,312.33/1,841.90)	115.32 (113.50/172.63)	1,462.31 (1,317.90/1,871.22)	906.63 (846.90/1,166.56)	2,881.08 (2,683.60/2,959.72)
8th week	1	3	213.90 (207.89/239.38)	25.62 (22.09/29.98)	214.88 (207.62/241.09)	131.95 (119.36/144.10)	778.54 (701.23/975.66)
	2		1,494.03 (1,405.20/2,328.37)	104.23 (100.65/178.85)	1,496.15 (1,410.31/2,334.36)	1,097.21 (991.52/1,393.91)	2,455.46 (2,189.75/4,101.60)

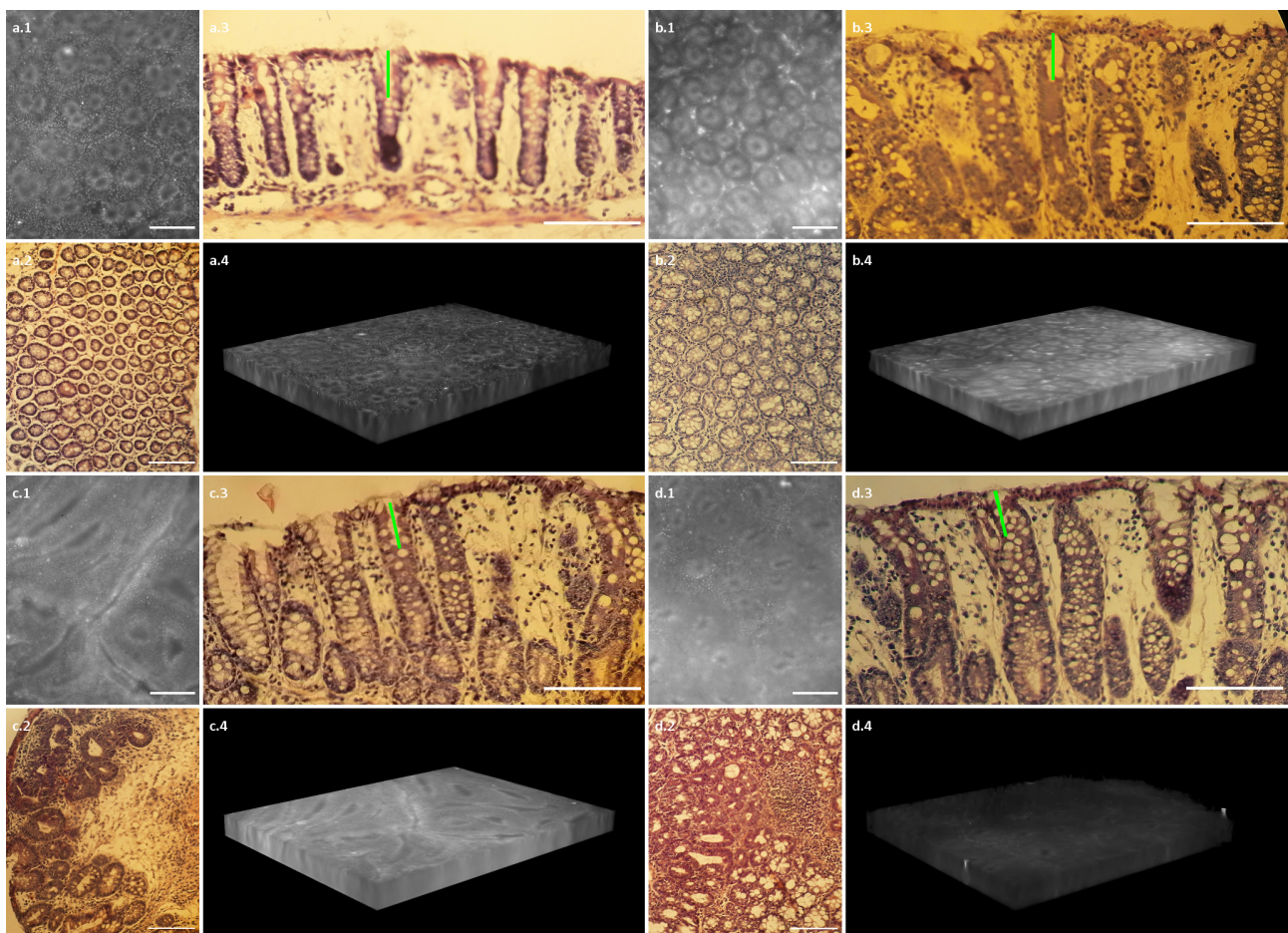


FIGURE 2. H&E sections and autofluorescence images for control samples (A) and for CRC development at 2nd, 4th, and 8th weeks after AOM/DSS induction (B, C, D). Transverse sections (A/B/C/D.1, A/B/C/D.2) of the distal colon mucosa views from autofluorescence and H&E-stained paraffin sections. H&E longitudinal sections (A/B/C/D.3) pointing out (50 µm green line) the equivalent length in Z-axis of the analysed autofluorescence volume. 3D autofluorescence images (a/b/c/d.4) oriented from the superficial mucosa to the inner layers. Scale bars: 100 µm.

shape and columnar orientation can be observed in longitudinal views of H&E sections.

Autofluorescence quantification and characterization

Median and interquartile ranges for each measure are summarized in TABLE 1, which provides details about the number of images used for the quantification, the experimental study number, and the corresponding time point. The barplots of FIGURE 3 depict statistically significant differences in the mean.

The median values reveal that the autofluorescence intensity is relatively homogeneous in control animals but becomes highly heterogeneous in those induced to develop CRC. In most of the samples, the intensity and variability of the fluorescence decreased at initial stages (2nd week) compared to the control samples. However, in the 4th and 8th weeks the autofluorescence behaviour became more challenging to characterize. As normal tissue progressed toward neoplasia, the intensity exhibited an increment or a considerable reduction in its value compared to control and the 2nd week of induction. This heterogeneity is exemplified in the volumes in FIGURE 3 and also in FIGURE 4, in which is represented the summed slices projections of the image stacks from the first experimental study.

In statistical terms, significant differences were detected for the mean, SD and minimum parameters only between samples from control and those from the 2nd week, concerning the 4th week of the first experimental study (FIGURE 3).

DISCUSSION

Flavins such as riboflavin (vitamin B2), flavin adenine dinucleotide (FAD) and flavin mononucleotide (FMN), as well as lipopigments such as lipofuscins, are the endogenous fluorophores located at the mucosa^(10,18,33,34) that contribute to the autofluorescence signal captured at a thickness of approximately 50 μm , starting from the luminal surface of the colonic mucosa, employing the optical system setting described in the Image acquisition section from Methods. Based on this and having successfully validated the correlation between histological and autofluorescence changes in the data sets, we proceeded to define

specific intensity features to characterize the autofluorescence based on the performed quantification.

The high heterogeneity exhibited by the median values in the emission properties of the samples from induced animals developing CRC is expected, given that autofluorescence is highly sensitive to alterations in tissue morphology and biochemistry resulting from malignant transformation⁽¹⁴⁾. Furthermore, the morphological and metabolic conditions of cells and tissues strictly influence the nature, amount, physicochemical state, intra-tissue distribution, and microenvironment of the endogenous fluorophores⁽¹⁰⁾.

The statistical evidence suggested that as most of the differences between normal and CRC samples were not statistically significant, the latter could be linked to hyperplastic tissue based on DaCosta et al.^(14,15) characterization of normal, hyperplastic, and adenomatous tissue autofluorescence^(14,15). In that study, it is reported that the fluorescence is the same for epithelial cells from the first two categories. This result is not unexpected considering that hyperplastic epithelia are similar to normal epithelia in phenotype, differentiation, and maturity⁽¹⁴⁾.

Regarding the heterogeneity of the intensity in CRC samples, on the one hand, it is well known that dysplastic epithelial cells from adenomatous polyps have more fluorescent granules heterogeneously distributed in the lamina propria and in apical regions of the epithelia^(14,15). Thus, the detected fluorescence intensity is often higher than normal and hyperplastic cells. Furthermore, it is postulated that additional factors, such as an increased number of mitochondria and/or lysosomes per cell, changes in total cell volume, variations in relative fluorophore concentrations, and/or inherent shifts in their molecular conformation(s) of fluorophores, their oxidation and reduction states, and/or their free or bound forms, may contribute to the variability observed in the resulting intensities^(14,15). On the other hand, the review conducted by the Ramanujam et al.⁽³³⁾ on fluorescence microscopy and spectroscopy of micro-structures in tissue sections suggests that despite obtaining varying results, there are notable differences in signal intensity between normal and neoplastic specimens. The intensity was mainly increased in dysplastic cells of hyperplastic or adenomatous polyps relative to the normal (although the other way was also

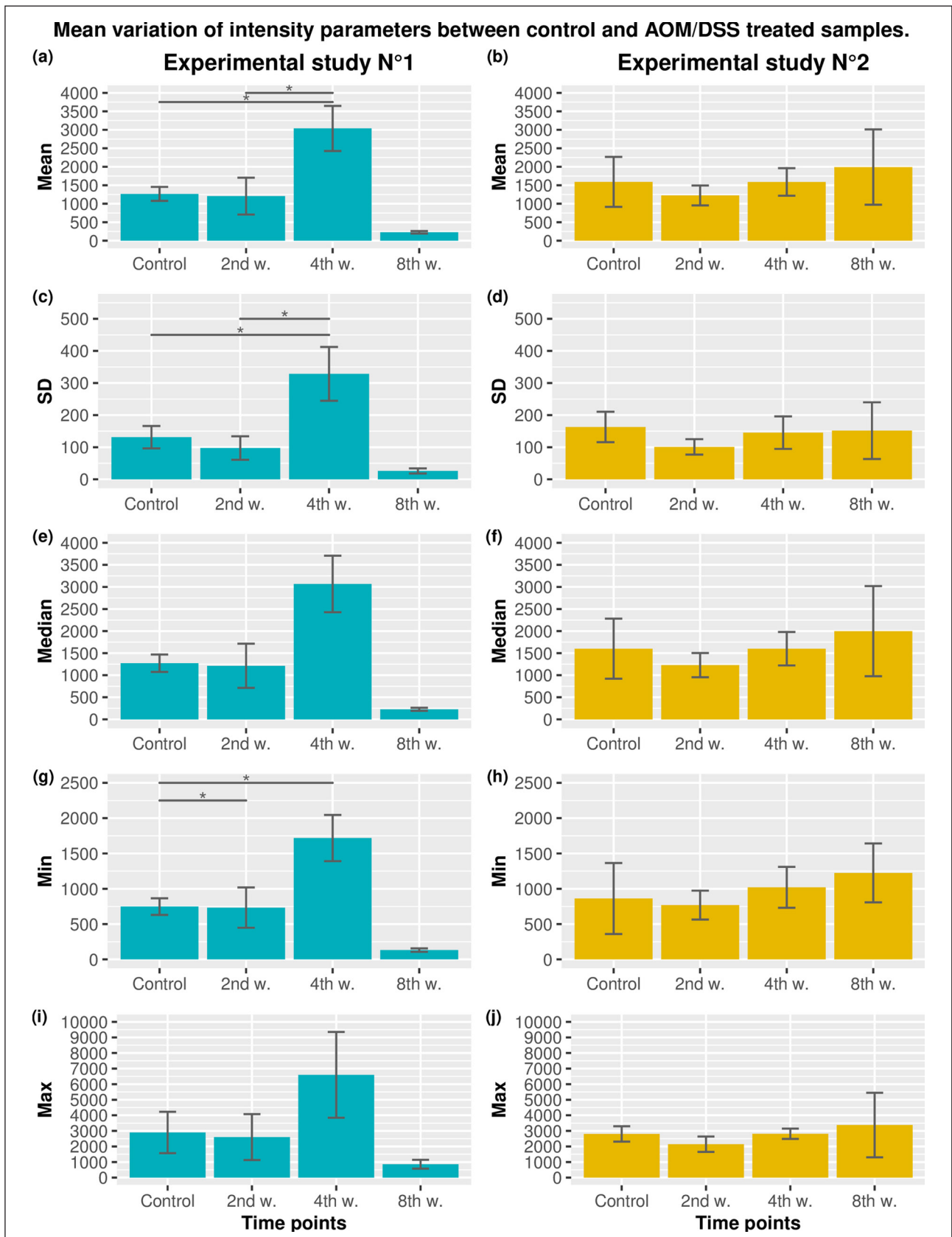


FIGURE 3. Barplots with error bars and SD for mean values of mean (A, B), SD (C, D), median (E, F), minimum (G, H), and maximum (I, J). Significance was noted (*) for P -values <0.05 and (**) for P -values <0.01 .

reported). Conversely, it demonstrated a decrease in adenocarcinomas compared with adenomas. Hence, the significant increment observed in the 4th week is supported by the majority of the aforementioned findings and the corresponding samples could be linked to hyperplastic or adenomatous tissues, according to Ramanujam et al.⁽³³⁾ and DaCosta et al.⁽¹⁴⁾.

In summary, it can be inferred that control samples from the first experimental study come from normal mucosa, whereas the samples from the 2nd and 4th weeks likely come from hyperplastic and adenoma tissue, respectively. While the intensity reduction in the 8th week samples relative to the previous week values suggests a link to adenocarcinoma, the lack of statistical significance leads to their classification as hyperplastic as well. The second experimental study did not reveal significant differences for all the analysed parameters. However, considering that three of the time points analysed are pathological, it is possible to infer that all of them come from hyperplastic tissue. Alternatively, the lack of significant differences could be due to the sample size not being sufficient to detect intensity variations arising from adenoma or adenocarcinoma.

Based on the statistical analyses, it can be noted that the CRC features could be detected after the 2nd week post-induction and, in a preliminary manner, the samples of the time points involved in the progression process to CRC were characterized. However, further work is needed to enhance the accuracy of the autofluorescence intensity characterization for each pathological time point.

CONCLUSION

In conclusion, we conducted a 3D intensity quantification on volumes of approximately 50 μm of the colon mucosa using fresh murine colon tissue samples. This quantification allowed for an autofluorescence characterization at the 2nd, 4th and 8th weeks after CRC induction by AOM/DSS. The characterization was achieved through software processing and

analysis of widefield autofluorescence microscopy image stacks. The results pointed out that the intensity is comparable in non-pathological samples, but it undergoes remarkable changes during the progression of the tumor process. Furthermore, the statistically significant differences found allowed to characterize the early evolution of CRC, particularly after the 2nd week post-injection using a well-established murine model of CRC.

Optical biopsy is an ongoing developing non-invasive technology that aims to address and support biomedical diagnostic procedures. However, the use of autofluorescence still presents challenges due to levels of variability that hinder a more comprehensive systematization of the data obtained during the progression of CRC. In context, this study should be acknowledged as a significant step forward towards non-invasive and rapid diagnostic methods. Future research will aim to replicate the study enhancing the analysis accuracy and providing a more precise description of the intensity of samples coming from dysplasia to CRC.

ACKNOWLEDGMENTS

The authors would like to thank Professor Diana Waigandt for her valuable assistance in the English language editing of the manuscript.

Authors' contribution

Erbes LA: design and execution of the experimental studies, image acquisition, design and execution of the image digital processing methodology, statistical data analysis and writing the manuscript. Casco VH: reviewing the manuscript. Adur J: design and execution of the experimental studies, data analysis, and reviewing the manuscript.

Orcid

Luciana Ariadna Erbes: 0000-0003-3632-136X.

Víctor Hugo Casco: 0000-0002-3737-479X.

Javier Adur: 0000-0003-2176-2226.

Erbes LA, Casco VH, Adur J. Caracterização dos estágios iniciais do câncer colorretal utilizando microscopia de autofluorescência 3D: um estudo preliminar. *Arq gastroenterol.* 2024;61:e23062.

RESUMO – Contexto – O câncer colorretal é uma das patologias mais prevalentes em todo o mundo, cujo prognóstico está ligado à detecção precoce. A colonoscopia é o padrão ouro para triagem, e o diagnóstico geralmente é feito histologicamente a partir de biópsias. Visando reduzir o tempo de inspeção e diagnóstico, bem como as biópsias e recursos envolvidos, outras técnicas estão sendo promovidas para realizar avaliações precisas de colonoscopia in vivo. A biópsia óptica visa detectar tecidos normais e neoplásicos analisando o espectro de autofluorescência com base nas mudanças na distribuição e concentração de moléculas autofluorescentes causadas pelo câncer colorretal. Portanto, a contribuição da autofluorescência analisada por técnicas de processamento de imagem poderia ser uma abordagem para uma caracterização mais rápida do tecido-alvo. **Objetivo** – Quantificar parâmetros de intensidade por meio do processamento digital de dois conjuntos de dados de imagens de microscopia de autofluorescência em campo amplo tridimensionais, adquiridas por amostras de tecido fresco de cólon de um modelo murino de câncer colorretal. Adicionalmente, analisar os dados de autofluorescência para fornecer uma caracterização em um volume de aproximadamente 50 µm da mucosa do cólon para cada imagem, na segunda (2ª), quarta (4ª) e oitava (8ª) semanas após a indução do câncer colorretal. **Método** – Desenvolvimento de um modelo murino de câncer colorretal usando indução de azoximetano/sulfato de sódio dextrano, e aquisição de conjuntos de dados de imagens Z-stack por microscopia de autofluorescência em campo amplo, de animais controle e induzidos ao câncer colorretal. Etapas de pré-processamento de ajustes de valores de intensidade seguidas por procedimentos de quantificação e caracterização usando automação de fluxo de trabalho de processamento de imagem por macros do Fiji, e análise estatística de dados. **Resultados** – A eficácia do modelo de indução de câncer colorretal foi corroborada por uma avaliação histológica para correlacionar e validar a ligação entre as mudanças histológicas e de autofluorescência. A metodologia de processamento digital de imagem proposta foi então realizada nas imagens tridimensionais de camundongos controle e das 2ª, 4ª e 8ª semanas após a indução química do câncer colorretal, para cada conjunto de dados. Análises estatísticas encontraram diferenças significativas nos parâmetros médios, desvio padrão e mínimos entre amostras de controle e aquelas da 2ª semana após a indução em relação à 4ª semana do primeiro estudo experimental. Isso sugere que as características do câncer colorretal podem ser detectadas após a 2ª semana pós-indução. **Conclusão** – O uso de autofluorescência ainda apresenta níveis de variabilidade que impedem uma maior sistematização dos dados obtidos durante a progressão do câncer colorretal. No entanto, esses resultados preliminares podem ser considerados uma abordagem para a caracterização tridimensional da autofluorescência do tecido colorretal, descrevendo as características de autofluorescência de amostras que vão da displasia ao câncer colorretal.

Palavras-chave – Autofluorescência; câncer colorretal; processamento de imagem; microscopia.

REFERENCES

1. De-Souza AS, Costa-Casagrande TA. Animal models for colorectal cancer. *Arq Bras Cir Dig.* 2018;31:1-4.
2. Sung H, Ferlay J, Siegel RL, Laversanne M, Soerjomataram I, Jemal A, et al. Global cancer statistics 2020: Globocan estimates of incidence and mortality worldwide for 36 cancers in 185 countries. *CA: A Cancer J Clin.* 2021;71:209-49.
3. Brenner H, Kloor M, Pox CP. Colorectal cancer. *The Lancet.* 2014;383:1490-502.
4. Prasad M, Lalme U, Ranjan K, Patil S, Brar B, Devi B, et al. An Insight in Biomarkers for Colorectal Cancer. *J Gastroenterol Liver Dis.* 2018;3:1-15.
5. Facciorusso A, Antonino M, Di Maso M, Barone M, Muscatiello N. Non-polypoid colorectal neoplasms: Classification, therapy and follow-up. *World J Gastroenterol.* 2015;21:5149-57.
6. Yoshioka S, Mitsuyama K, Takedatsu H, Kuwaki K, Yamauchi R, Yamasaki H, et al. Advanced endoscopic features of ulcerative colitis-associated neoplasias: Quantification of autofluorescence imaging. *Int J Oncol.* 2016;48:551-8.
7. Glover B, Teare J, Patel N. The status of advanced imaging techniques for optical biopsy of colonic polyps. *Clin Transl Gastroenterol.* 2020;11:1-11.
8. Van Den Broek FJ, Van Soest EJ, Naber AH, Van Oijen AH, Mallant-Hent RC, Böhrer CJ, et al. Combining autofluorescence imaging and narrow-band imaging for the differentiation of adenomas from non-neoplastic colonic polyps among experienced and non-experienced endoscopists. *Am J Gastroenterol.* 2009;104:1498-1507.
9. Li Y. Separation of endogenous fluorophores in normal and cancer cells [PhD thesis]. [Iowa City, IA]: University of Iowa; 2009.
10. Croce AC, Bottiroli G. Autofluorescence spectroscopy and imaging: A tool for biomedical research and diagnosis. *Eur J Histochem.* 2014;58:320-37.
11. Deal J, Mayes S, Browning C, Hill S, Rider P, Boudreaux C, et al. Identifying molecular contributors to autofluorescence of neoplastic and normal colon sections using excitation-scanning hyperspectral imaging. *J Biomed Opt.* 2018;24:1-11.
12. Kominami Y, Yoshida S, Tanaka S, Miyaki R, Sanomura Y, Seo MW, et al. Evaluation of dual-wavelength excitation autofluorescence imaging of colorectal tumours with a high-sensitivity CMOS imager: A cross-sectional study. *BMC Gastroenterology.* 2015;15:1-6.
13. Van Den Broek FJC, Fockens P, Van Eeden S, Reitsma JB, Hardwick JCH, Stokkers PCF, et al. Endoscopic tri-modal imaging for surveillance in ulcerative colitis: randomised comparison of high-resolution endoscopy and autofluorescence imaging for neoplasia detection; and evaluation of narrow-band imaging for classification of lesions. *Gut.* 2008;57:1083-9.
14. Dacosta RSL. Mechanisms of fluorescence endoscopy of the human colon [MSc thesis]. [Ottawa]: National Library of Canada; 2000.
15. Dacosta RS, Andersson H, Cirocco M, Marcon NE, Wilson BC. Autofluorescence characterisation of isolated whole crypts and primary cultured human epithelial cells from normal, hyperplastic, and adenomatous colonic mucosa. *J Clin Pathol.* 2005;58:766-74.
16. Borisova E, Genova T, Bratashov D, Lomova M, Terziev I, Vladimirov B, et al. Macroscopic and microscopic fluorescence spectroscopy of colorectal benign and malignant lesions - diagnostically important features. *Biomed Opt Express.* 2019;10:3009-17.
17. Thia KT-J, Kong CS-C, Ooi C-J. Narrow band imaging and autofluorescence imaging for the detection and optical diagnosis of colorectal polyps. *Proceedings of Singapore Healthcare.* 2010;19:51-6.
18. Ghukasyan VV, Heikal AA. Natural biomarkers for cellular metabolism: Biology, techniques, and applications. Boca Raton: CRC Press. 2015.

19. Rosenberg DW, Giardina C, Tanaka T. Mouse models for the study of colon carcinogenesis. *Carcinogenesis*. 2009;30:183-96.
20. Erbes LA, Izaguirre MF, Casco VH, Adur J. Three-dimensional morphological characterization of colorectal pits from label-free microscopy images. *MRT*. 2022;85:1937-48.
21. National Research Council. *Guide for the Care and Use of Laboratory Animals*. Washington: The National Academies Press; 2011.
22. Schindelin J, Arganda-Carreras I, Frise E, Kaynig V, Longair M, Pietzsch T, et al. Fiji: an open source platform for biological image analysis. *Nat Methods*. 2012;9:676-82.
23. Miura K. Bleach correction ImageJ plugin for compensating the photobleaching of time-lapse sequences. *F1000Research*. 2020;9:1-17.
24. Sage D, Donati L, Soulez F, Fortun D, Schmit G, Seitz A, et al. Deconvolutionlab2: An open-source software for deconvolution microscopy. *Methods*. 2017;115:28-41.
25. Widefield fluorescence microscope PSF [Internet]. Icy. Available from: <http://icy.bioimageanalysis.org/plugin/widefield-fluorescence-microscope-psf/>
26. de Chaumont F, Dallongeville S, Chenouard N, Hervé N, Pop S, Provoost T, et al. Icy: an open bioimage informatics platform for extended reproducible research. *Nat Methods*. 2012;9:690-6.
27. Pang Z, Laplante NE, Filkins RJ. Dark pixel intensity determination and its applications in normalizing different exposure time and autofluorescence removal. *J Microsc*. 2012;246:1-10.
28. Pang Z, Filkins RJ. Methods for scaling images to differing exposure times United States Patent Patent No: US 8,818,069 B2. 2014.
29. Hamamatsu. ORCA FLASH 2.8 Technical Note. Japan: Hamamatsu Photonics K K, Systems Division; 2011.
30. National Institutes of Health. U.S. Department of Health and Human Services [Internet]. Measure - Analyze Menu. Available from: <https://imagej.nih.gov/ij/docs/menus/analyze.html#measure>
31. Tan CW, Hirokawa Y, Gardiner BS, Smith DW, Burgess AW. Colon cryptogenesis: asymmetric budding. *PLoS One*. 2013;8:1-18.
32. RStudio [Internet]. Rstudio: Integrated Development Environment for R. 2023. Available from: <http://www.rstudio.com/>
33. Ramanujam N. Fluorescence spectroscopy of neoplastic and non-neoplastic tissues. *Neoplasia*. 2000;2:89-117.
34. Li L, Li H, Chen Z, Zhuo S, Feng C, Yang Y, et al. Layer-resolved colorectal tissues using nonlinear microscopy. *Lasers Med Sci*. 2015;30:1589-97.